THE JOURNAL OF PHYSICAL CHEMISTRY C

Article

pubs.acs.org/JPCC

Photoelectrochemical and Electrochemical Characterization of Sub-Micro-Gram Amounts of Organic Semiconductors Using Scanning Droplet Cell Microscopy

Jan Philipp Kollender,[†] Jacek Gasiorowski,[‡] Niyazi S. Sariciftci,[‡] Andrei I. Mardare,[†] and Achim Walter Hassel*[,†,§]

[†]Institute for Chemical Technology of Inorganic Materials, [‡]Linz Institute for Organic Solar Cells (LIOS), Physical Chemistry, and [§]Christian Doppler Laboratory for Combinatorial Oxide Chemistry at the Institute for Chemical Technology of Inorganic Materials, Johannes Kepler University Linz, Altenberger Str. 69, 4040 Linz, Austria

ABSTRACT: A model organic semiconductor (MDMO-PPV) was used for testing a modified version of a photoelectrochemical scanning droplet cell microscope (PE-SDCM) adapted for use with nonaqueous electrolytes and containing an optical fiber for localized illumination. The most attractive features of the PE-SDCM are represented by the possibility of addressing small areas on the investigated substrate and the need of small amounts of electrolyte. A very small amount (ng) of the material under study is sufficient for a complete electrochemical and photoelectrochemical characterization due to the scanning capability of the cell. The electrochemical behavior of the polymer was studied in detail using potentiostatic and potentiodynamic investigations as well as electrochemical impedance spectroscopy. Additionally, the photoelectrochemical properties were investigated under illumination conditions, and the photocurrents found were at least 3 orders of magnitude higher than the dark (background) current, revealing the usefulness of this compact microcell for photovoltaic characterizations.

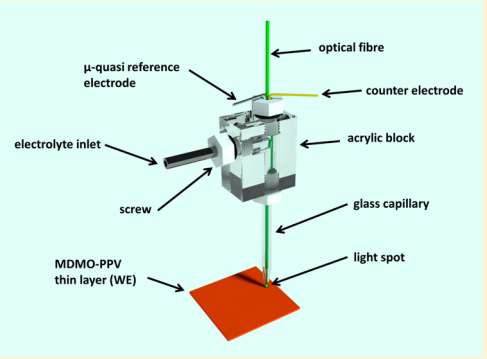

1. INTRODUCTION

The development of inexpensive and efficient photovoltaic devices is still a topic of high scientific importance. The vast majority of today's commercially available photovoltaic elements are based on inorganic semiconductors. The impressive advancements in the field of organic semiconductors within the last two decades have introduced the realistic potential for a much cheaper way to produce electrical energy from light.[1] Organic semiconductors combine the general properties of semiconductors with the easy processability of organic molecules, while manufacturing of solar cells based on inorganic semiconductors still requires high vacuum-based coating processes.[2,3] Thin-film photovoltaic devices based on organic semiconductors can be easily printed on lightweight, rugged, and flexible substrates.[4−8] Another clear advantage of organic semiconductors is the possibility to chemically modify the material properties. Additionally, the electronic structure of organic semiconductors can be relatively easy modified by changing the molecular structure via chemical synthesis.[9−11] In contrast to all these advantages, the initial synthesis of new organic semiconductors is a time-consuming and expensive process.

A large number of physical and chemical properties of organic semiconductors can be investigated by electrochemical and photoelectrochemical measurements.[12,13] The doping level of organic semiconductors can be randomly changed through electrochemical processes. The degree of electrochemical doping may be monitored via electrochemical impedance spectroscopy (EIS).[12,14,15] Cyclic voltammetry offers an appropriate way to determine the position of HOMO and LUMO levels of organic semiconductors.[13,16] Various other in situ spectroscopic methods have been developed to study optical and electronic changes induced by electrochemical processes.[17−21] However, for all of them, individual samples need to be prepared which is a rather time and material-consuming process. Photoinduced currents under various different redox conditions can be easily studied by photo-electrochemistry. In addition, concurrent or subsequent processes such as photodegradation or photodoping can be investigated using photoelectrochemistry.[22]

Even when only partially studying the electrochemical and photoelectrochemical properties, different samples and overall relatively big amounts of material are required. Therefore, finding a way of drastically decreasing the amount of material required for investigation is highly relevant. One attempt is based on a strong miniaturization of the area addressed by the electrochemical cell, which automatically leads to a drastic reduction of the amount of material to be consumed. This approach can be realized by, for example, photoelectrochemical scanning droplet cell microscopy (PE-SDCM), as it is capable

Special Issue: Michael Grätzel Festschrift

Received: January 14, 2014
Revised: May 12, 2014
Published: May 19, 2014

   dx.doi.org/10.1021/jp500423a | J. Phys. Chem. C 2014, 118, 16919−16926

of performing all common photoelectrochemical and electrochemical techniques on a single substrate.[6] The central idea behind PE-SDCM is that only a small electrolyte droplet released from the tip of a capillary with a small inner diameter comes into contact with the sample surface that is acting as the working electrode (WE).

In this paper, a modified version of a PE-SDCM adapted for use with nonaqueous electrolyte solutions is presented and tested under different conditions. The photoelectrochemical properties of a thin film of poly[2-methoxy-5-(3′,7′-dimethyloctyloxy)-1,4-phenylenevinylene] (MDMO-PPV), which is a model PPV-based donor organic semiconductor, was studied in detail.[23] Recently, the doping effect on the optical properties of MDMO-PPV was reported.[24] Although its applicability in photovoltaic devices was already shown, no detailed photoelectrochemical characterization of this material was done up to now. Using the PE-SDCM, all common electrochemical and photoelectrochemical experiments were performed on spot sizes of less than 0.04 mm^2. The user can easily switch between electrochemical and photoelectrochemical experiments without having to change the cell or the substrate. Using PE-SDCM, more than 100 electrochemical experiments on individual spots could be performed on a single 15 × 15 mm^2 substrate consuming less than 2 mL of electrolyte. All experiments can be performed in a two or three electrode configuration. Performing such a large number of experiments on a single substrate drastically reduces the amount of consumed material, reduces the time for sample preparation, and eliminates possible variations between different samples. Also, different light sources like lasers, LEDs, or halogen lamps can be used to meet various experimental requirements.

2. EXPERIMENTAL SECTION

2.1. Preparation of Polymer Thin Film Samples. To demonstrate the measurement capabilities of PE-SDCM for electrochemical and photoelectrochemical characterization of organic semiconductors under nonaqueous conditions, a thin film of poly[2-methoxy-5-(3′,7′-dimethyloctyloxy)-1,4-phenylenevinylene] (MDMO-PPV; Covion GmbH, Frankfurt, Germany) was used. The structure of the polymer is presented in Figure 1. At first, the organic semiconductor was dissolved in

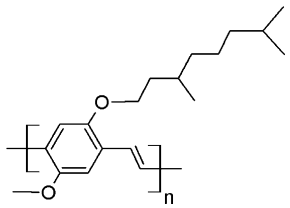

Figure 1. Chemical structure of MDMO-PPV.

pyridine (99+%, Alfa Aesar) with a concentration of 10 g L^{-1}. The thin film used for electrochemical characterization was prepared by spin-casting the dissolved polymer molecules onto a precleaned 15 × 15 mm^2 ITO/glass slide (15 Ω sq^{-1}, Kintec Co.) The glass/ITO substrate was cleaned by consecutive sonication in isopropanol, acetone and deionized water. The film thickness was measured using a DekTak XT Stylus profilometer (Bruker Corp., U.S.A.).

2.2. Fabrication of PE-SDCM. All electrochemical and photoelectrochemical measurements shown in this publication were carried out using a special photoelectrochemical scanning droplet cell microscope adapted for the use of nonaqueous, organic-based electrolytes. The main body of the cell was made from an acrylic block (22 mm × 22 mm × 12 mm) into which three connected channels (3.3 mm in diameter) were drilled (see Figure 2). Each channel was sealed using polypropylene

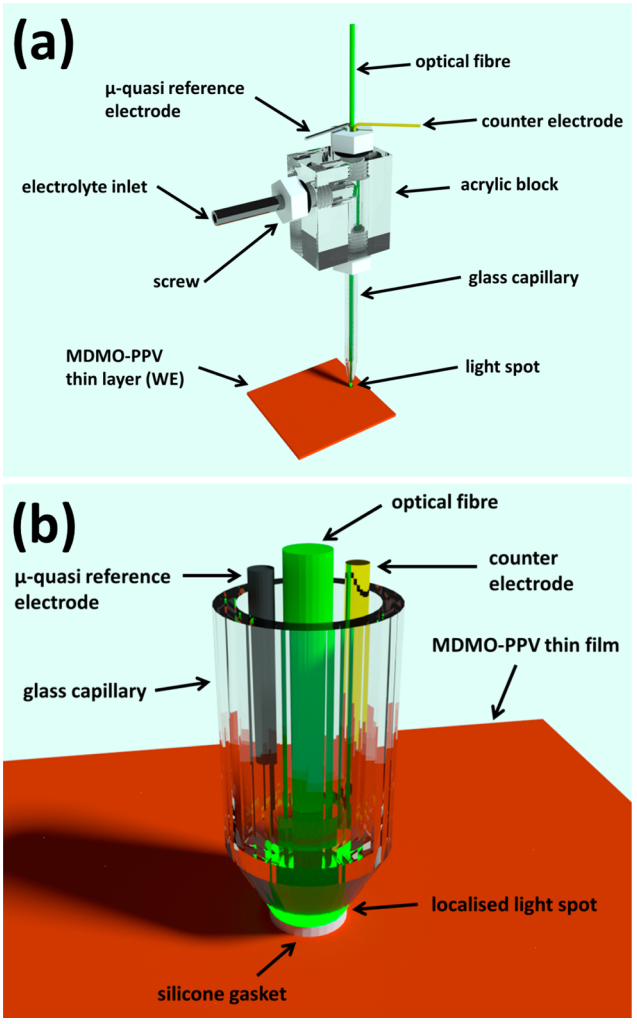

Figure 2. Scheme of the photoelectrochemical scanning droplet cell microscope (PE-SDCM).

(PP) screws with an O-ring underneath the head of each screw. A μ-Ag/AgCl system adapted for use in organic-based solvents was used as a micro quasi reference electrode (μ-QRE). The potential sensitive part of the μ-QRE was prepared by electrodeposition of AgCl on the first 10 mm of a longer 100 μm in diameter Ag wire in 1 M HCl. A detailed description of the deposition process can be found elsewhere.[25] The partially coated wire was inserted into a small glass capillary for increased mechanical stability, leaving the potential sensing part exposed outside it. To avoid contact between the uncoated part of the Ag wire and electrolyte, the glass capillary was sealed on both ends using two component epoxy resin (UHU GmbH, Germany). This leads to increased mechanical stability of the μ-QRE and avoids possible cross contaminations. The potential of this electrode was 0.211 V versus standard hydrogen electrode (SHE). The counter electrode (CE) used for the PE-SDCM was made from a flattened 100 μm in diameter Au wire (99.999%, Wielandt Dentaltechnik, Germany). Flattening of

dx.doi.org/10.1021/jp500423a | J. Phys. Chem. C 2014, 118, 16919−16926

the Au wire increases the surface area of the CE and results in a high CE/WE surface ratio.

The lower part of the PE-SDCM, from which the droplet is released, was made from a borosilicate glass capillary with an outer diameter of 2.5 mm. It was tailored using a commercial capillary puller (PC-10, Narishige, Tokyo, Japan). The size of the tip was adjusted to the final desired size using an in-house developed capillary polisher equipped with 2400 and 4000 grade SiC sandpaper (Struers A/S, Ballerup, Denmark). After polishing, the glass tube was thoroughly cleaned with acetone and isopropanol, followed by deionized water, and blown dry using nitrogen. A silicone seal was formed at the rim of the capillary by dipping it into liquid silicone (RTV, Momentive, Albany, U.S.A.) and dried under constant nitrogen flow for several hours. This gasket allows operation of the PE-SDCM in contact mode, where the tip of the cell is pressed against the surface of the sample. This approach leads to a very high reproducibility of the area addressed by the PE-SDCM due to confinement of the electrolyte droplet within the inner volume defined by the silicone sealing. Additionally, such a sealing strongly reduces contamination of the electrolyte (e.g., water) by eliminating direct exposure of the electrolyte to the atmosphere during measurements.

Next, this capillary was mounted in a screw allowing an easy way of fixing it to the acrylic block. In order to locally illuminate the area addressed by the PE-SDCM, a 270 μm multimode optical fiber was used. The length of the fiber, RE and CE were chosen in such a way that all three, when installed inside the tip capillary, are in close proximity to the surface (see Figure 2b). This ensures homogeneous illumination of the wetted area and minimizes potential drop between RE and sample surface (WE). Inside a third screw a 800 μm in diameter stainless steel capillary was installed using a two-component epoxy glue (UHU GmbH, Germany). This capillary was used as electrolyte inlet and was connected via a Teflon tube to a high-precision syringe pump (World Precision Instruments, U.S.A.). The pump served as an electrolyte reservoir and was additionally used to precisely control the size of the electrolyte droplet formed at the tip of the capillary. To determine the area wetted by the PE-SDCM, a sputter deposited Ti thin film was anodized in an aqueous 0.1 M Na_2SO_4 solution.[8] The area of the colored oxide spot was determined using an automated optical pattern recognition software (NIS Elements D, Nikon, Japan).

2.3. Illumination Sources. All photoelectrochemical experiments presented in this work were performed using a 532 nm, diode pumped solid state laser module with built-in auto power control. This specific wavelength was chosen to match the absorption maximum of MDMO-PPV, which was determined by spectroscopic ellipsometry (SE). Details about this can be found elsewhere.[9] Various different light sources, for example, high-power LEDs, UV/vis continuum emitters, monochromators with optical fiber output, and different kinds of lasers have already been successfully used with PE-SDCM.[6] The 532 nm laser was coupled externally into the fiber using an in-house developed fiber port. To avoid any disturbance of the measurements by ambient light sources, all experiments were carried out in a specially designed dark room. The intensity of the light source was adjusted by using a gray-shade filter (Thorlabs, U.S.A.) positioned midway between laser source and fiber port. Blockage of the laser beam was done by means of a manually operated shutter. To determine the optical power density on the area addressed by the PE-SDCM, a fully assembled PE-SDCM was positioned on the detector window of an optical power meter (Coherent Lasermate Q). The measured optical power density was 153 mW cm^{-2}.

2.4. Electrochemical and Photoelectrochemical Measurements. The PE-SDCM was positioned on the sample surface in a fully automated fashion using a gantry robot build from three linear stages. For maximum reproducibility of the wetted area the PE-SDCM was operated in contact mode.[6] The applied force was continuously monitored using a small force sensor (ME-Messsysteme, Germany) and, if necessary, re-adjusted by feedback to the z-axis. The complete setup was controlled by an in-house developed LabView program. As electrolyte, a 0.1 M solution of tetrabutylammonium hexafluorophosphate ($TBAPF_6$, ≥99%, Fluka Analytical, U.S.A) dissolved in propylene carbonate (PC, 99.7%, Sigma-Aldrich) was used. The electrolyte was prepared and stored in a glovebox to avoid possible contaminations caused by, for example, oxygen or water. All experiments were carried out in a three-electrode configuration using a potentiostat with a built-in frequency response analyzer for electrochemical impedance spectroscopy (EIS) measurements (Compactstat, Ivium Technologies, The Netherlands).

3. RESULTS AND DISCUSSION

3.1. Cyclic Voltammetry Studies. In order to characterize the electrochemical properties of the MDMO-PPV, cyclic voltammetry was performed. Using this technique, detailed information about the oxidation/reduction processes as well as their kinetics can be obtained. First, cyclic voltammetry with different scan rates was done. To avoid any interaction, for each measurement, the PE-SDCM was moved to a different location, and measurements with scan rates of 1, 3, 10, 30, and 100 mV s^{-1} were performed on sequentially addressed spots. All these cycles are presented together in Figure 3 to allow a direct

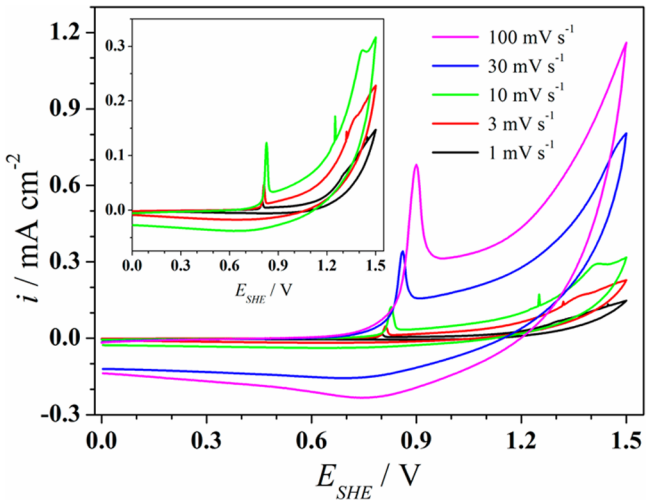

Figure 3. Scan rate dependent cyclic voltammetry on MDMO-PPV.

comparison. As can be seen, the observed maximum of the current density increases when increasing the scan rate, which can be easily explained by increased mass transport at higher scan rates. Due to the strong overlapping of the experimental data, the curves corresponding to the first three potential scan rates (up to 10 mV s^{-1}) are displayed separately in the inlet of Figure 3. Interesting observations can be done, if looking at the shape of the current−voltage curves as a function of the scan

dx.doi.org/10.1021/jp500423a | J. Phys. Chem. C 2014, 118, 16919−16926

rate. For scan rates up to 10 mV s^{-1} two oxidation peaks are found (see inlet Figure 3). For the first experiment with a scan rate of 1 mV s^{-1}, the oxidation peaks are found at 0.8 and 1.3 V. When increasing the speed of change of polarization up to 10 mV s^{-1}, the oxidation peaks are shifted to higher potentials. The lower potential oxidation peak shifts to 0.83 V, while the higher potential oxidation peak shifts to 1.44 V. The scan rate dependent peak position suggests a kinetic hindrance of the electrochemical oxidation process. As a result, higher potentials are needed for the same oxidation process to occur. Moreover, in all three experiments, no clear reduction peak could be observed, but instead, a very broad negative current distribution is noticeable. When comparing current−voltage characteristics measured with different polarization speeds, the different behavior of the reduction part of the voltammograms could be explained by a dissolution process of the previously oxidized MDMO-PPV, which becomes more significant at lower polarization speeds where a second oxidation peak was detected. For higher scan rates (30 and 100 mV s^{-1}), only one clear oxidation peak is found with a maximum at 0.86 and 0.9 V, respectively. As compared to the previously discussed case of low polarization speeds, the second oxidation peak is absent probably due to kinetic hindrance of the oxidation process. Additionally, for the high scan rate cases, a broad reduction peak centered at 0.8 V is observed.

In order to get a better understanding of the polymer oxidation and reduction processes, a series of cyclic voltammograms was measured with a scan rate of 10 mV s^{-1} on a single spot. In this experiment, the maximum potential was incrementally increased in steps of 0.05 V up to the final potential of 1.5 V. The results are plotted in Figure 4. During

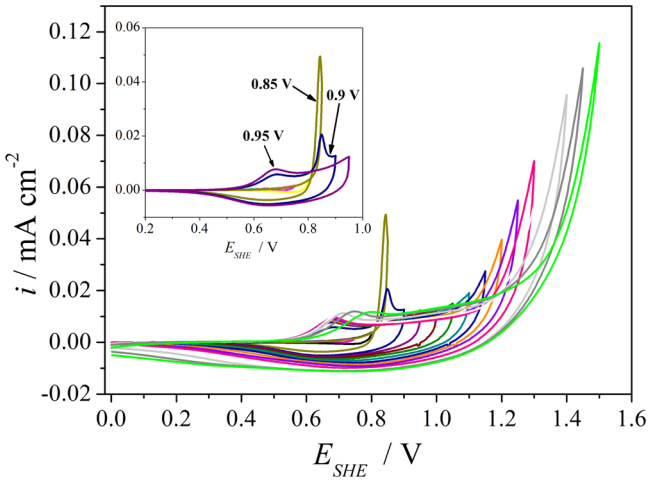

Figure 4. Cyclic voltammograms of MDMO-PPV for various reverse potentials. All scans with reverse potentials up to 1.5 V and scans with reverse potentials up to 0.95 V (inset).

experiments, all curves with the maximum potential up to 0.8 V, showed only background current. This is observable in the inlet of Figure 4, where only the first five experiments (with final potential up to 0.95 V) are presented. In the scan with a final potential of 0.85 V, a sharp and well-defined peak with maximum at 0.84 V, was found. In the next scan, with a final potential of 0.9 V the intensity of this peak reduces and a broadening can be observed. Additionally, a second anodic peak can now be observed at 0.68 V. The presence of this new peak is related to an initial oxidation of the MDMO-PPV. This peak was not measured before, probably due to the formation of an interfacial barrier on the polymer surface causing the previously discussed peak at 0.84 V. The next scan with a final potential of 0.95 V has only the initial oxidation peak centered at 0.68 V with a slightly higher current density than in the previous scan. For final potentials above 0.95 V, the peak characterizing the first oxidation step shifts toward higher potentials. The current density value at the peak maximum increases gradually up to 0.03 mA cm^{-2} in the case of the scan with the highest final potential. For the last three measured scans (1.4−1.5 V) the position of the first oxidation peak is shifted for about 50 mV up to 0.8 V for each additional experiment. For cyclic voltammograms with the final potential above 1 V, a strong increase in the current can be observed at the end of the anodic sweep. This peak can be related to a second oxidation step of the polymer. All performed cyclic voltammograms that show a clear Faradaic current have a rather undefined broad reduction peak. When increasing the maximum potentials of the scans, the maximum current density of the reductive current is shifted toward more positive potentials.

3.2. Potentiostatic Studies. Besides cyclic voltammetry, a series of potentiostatic experiments were performed. In this study the constant potential applied was increased stepwise. Within the entire measurement series, the addressed area of the MDMO-PPV layer was kept at the corresponding potential, while the resulting current was measured for 70 s. The obtained results are displayed as a 3D graph in Figure 5. In order to

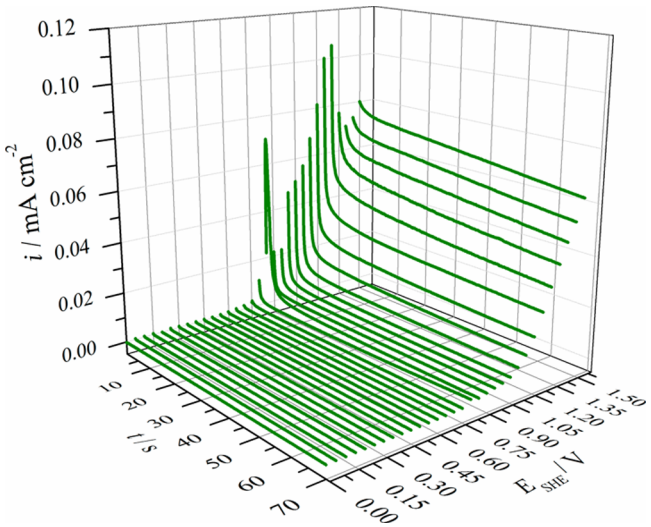

Figure 5. Time-dependent potentiostatic measurements on MDMO-PPV at different applied potentials.

obtain a more detailed description of the electrochemical processes caused by small changes in the applied potential, sufficiently small potential steps were used. A potential increase of 50 mV for each step was previously found to be suitable for investigating electrochemical doping of polymers and was used also for this study.[12]

For applied potentials below 0.75 V, only a background current density in the order of 10^{-4} mA cm^{-2} could be measured. The recorded current stays constant within the 70 s time frame of each measurement. In the potential range between 0.75−0.85 V, a defined oxidation is found. The increase in the current density is related to the oxidation of MDMO-PPV and to the potential corresponding to the

dx.doi.org/10.1021/jp500423a | J. Phys. Chem. C 2014, 118, 16919−16926

interfacial barrier previously discussed in the cyclic voltammetry studies. During the first 5 s of each potentiostatic measurement, a significant decrease in the current density can be observed, caused by the occurring electrochemical processes. At a later stage, the measured current density stabilizes into an almost constant plateau. When increasing the applied potential even further (above 0.85 V), the final current density measured after 70 s increases from one curve to the next. This effect can be explained by an increased conductivity of the oxidized organic semiconductor due to doping. As previously found, a significant decrease in current density within the first 5 s is observed. The magnitude of the onset current decrease (during the first 5 s) depends on the applied potential and gets significantly lower for the highest potentials.

A numerical integration of the potentiostatic curves presented in Figure 5 was performed in order to quantify the total charge taking part in the electrochemical processes at the semiconductor/electrolyte interface. This total charge is plotted as a function of the applied potential and the results are plotted in Figure 6 to allow for a further discussion of the

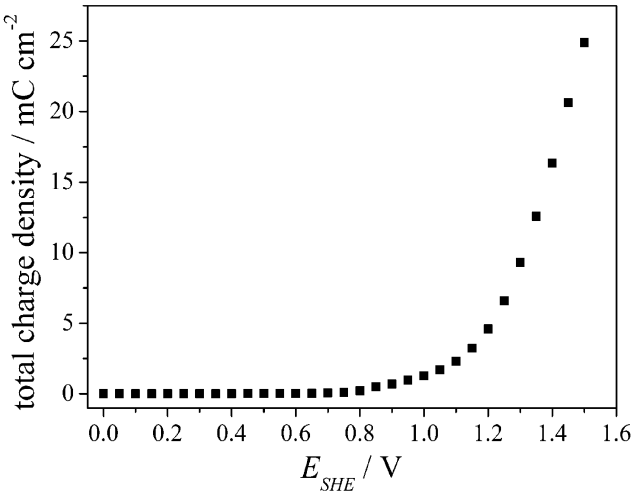

Figure 6. Total charge density measured on MDMO-PPV as a function of applied potential in the potentiostatic study.

electrochemical processes. Up to 0.75 V, a constant charge density of about 3 μC cm^{-2} is observed. This charge density is directly related to the background electrochemical current of the system. Similar to the previously discussed current transient experiments, at 0.85 V, a small oxidation is evidenced by a charge density increase. When increasing the potential further up to about 1.1 V, the charge density slowly increases up to about 0.6 mC cm^{-2}. For potentials between 1.1 and 1.4 V, an almost exponential growth of the charge density is observed. This charge density increase is mainly related to the second oxidation step of the MDMO-PPV, as observable in the fast decaying (within the first 5 s) current density curves plotted in Figure 5. As the applied potential increases from 1.4 to 1.5 V, the charge density increase can be also related to degradation processes. Additionally, the mentioned strong charge density increase is confirming the previously discussed electrochemical processes, which results in a conductivity increase of the MDMO-PPV due to the electrochemical oxidation. Overall, in the charge density dependence on the applied potential presented in Figure 6, no abnormal behavior of the system could be identified. This indicates long-term reliability of the PE-SDCM since the coulometric data is only confirming the electrochemical processes previously evidenced in the potentiostatic investigations from Figure 5.

3.3. Electrochemical Impedance Spectroscopy. In an attempt to study the electrical properties of the MDMO-PPV/electrolyte system, electrochemical impedance spectroscopy was performed using the PE-SDCM. Usually, conjugated polymers in their undoped form have insulating properties. Upon doping, their electrical properties can change drastically. Generally, at low doping levels they are considered as semiconductors. With increasing the doping level, their electrical resistance further decreases and they can show metal-like behavior. During the EIS study shown here, the frequency dependent changes of the impedance are monitored as a function of the applied DC bias (offset). Before each EIS experiment, a potentiostatic pretreatment was performed for 70 s in order to equilibrate the electrochemical processes. The used equilibration time of 70 s was chosen in agreement to the previous potentiostatic experiments, which showed a current density stabilization after this time interval (see Figure 5). All impedance spectra were recorded at a single addressed spot using sequentially increasing biases up to 1.4 V. After each spectrum, the bias was increased by 0.2 V and the frequency dependence of the impedance was determined again. In Figure 7, the corresponding Bode plots are shown in part (a) together with the associated phase shifts in part (b). As can be noticed, for biases below 0.6 V, there is no change in the shape and value of the impedance. In this bias range, the high frequency impedance suggests an electrolyte resistance of approximately 10^5 Ω. Similarly, the impedance value observable at the lowest frequency indicates a working electrode resistance in the order of 10^8 Ω. Starting with the applied bias of 0.6 V, a deviation of both the impedance and phase shift at low frequencies appears. This decrease is related to the oxidation of MDMO-PPV, resulting in an expected insulator-to-metal transition.[11] This decrease is continuing up to a bias of 1 V, where the working electrode impedance decreases by almost 2 orders of magnitude. In the same time, the phase shift changes substantially, finally reaching a value under −25°, observable at the middle of the investigated frequency range. At even higher applied potentials, an unexpected increase in the impedance can be observed. This effect can be related to dissolution of the oxidized MDMO-PPV layer, resulting in a change in the working electrode geometry.

3.4. Photoelectrochemical Studies. When a semiconductor is illuminated with light having an energy larger than the semiconductor bandgap, the energy of the photons can be absorbed and excited electrons and holes are generated in the conduction and valence band, respectively. When these photoexcited electrons or holes are in the space charge region they migrate toward the electrode surface where they participate in charge transfer reactions giving a photocurrent.[26] To demonstrate the functionality of PE-SDCM for photoelectrochemical measurements on organic semiconductors, photoinduced phenomena were studied on the MDMO-PPV film. The area addressed by the PE-SDCM was illuminated by the built-in optical fiber with a radiation of 532 nm wavelength (green) provided by an external laser. The wavelength of the radiation was chosen to match the maximum absorption of the polymer, as reported in a previous study.[25] Photocurrents caused by photogenerated electrons (cathodic currents) or holes (anodic current) are negligible when they are the majority charge carriers. Under these conditions, their concentration is

dx.doi.org/10.1021/jp500423a | J. Phys. Chem. C 2014, 118, 16919−16926

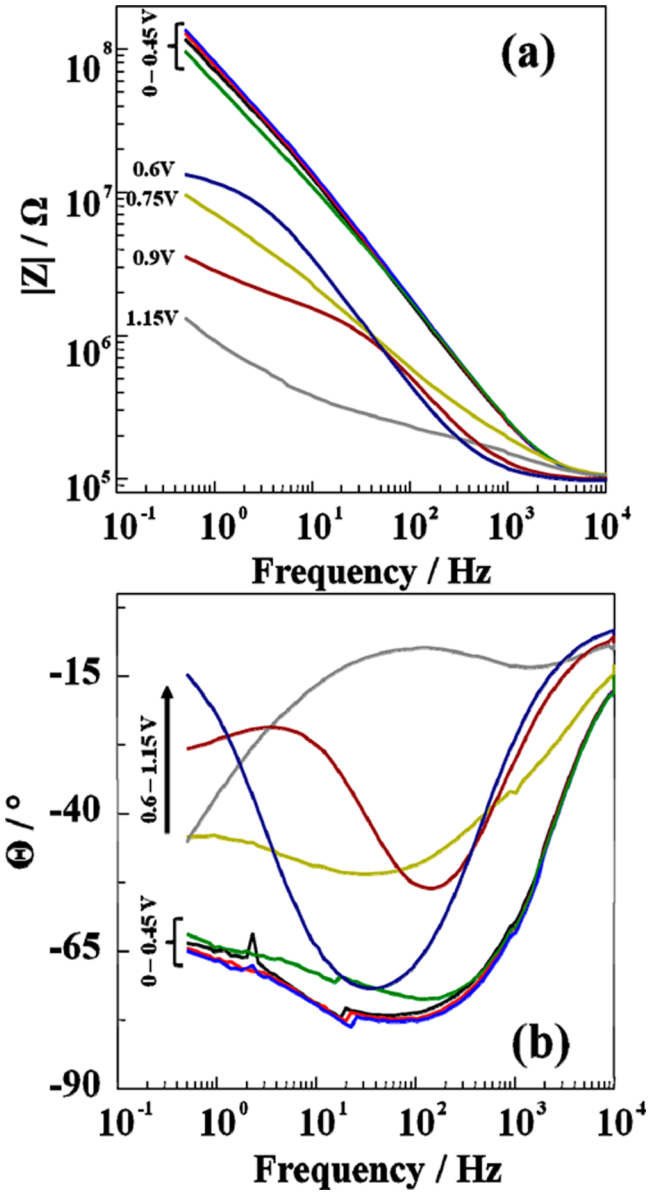

Figure 7. Impedance spectra measured on MDMO-PPV at different applied potentials.

barely increased by photoexcitation. However, their photocurrent becomes significant when the reacting electrons or holes are minority charge carriers. In this case their concentration is greatly increased by photoexcitation as compared with the concentration of the minority charge carriers in the absence of radiation (in the dark). Therefore, photocurrents can only be observed with reactions in which the participating carriers are minority charge carriers. This means transfer of holes at n-type electrodes and electrons at p-type electrodes leading to anodic and cathodic photocurrents, respectively.[27]

In Figure 8, photocurrent transients measured on MDMO-PPV under chopped light at different applied potentials are displayed. After approximately 10 s in the dark, the polymer was irradiated for another 10 s, defining one exposure cycle. In total, four exposure cycles were performed for applied potentials of 0.0, 0.2, and 0.4 V. For all potentials, the material is acting as a photocathode under illumination, which is a clear proof of the p-type nature of this polymer. Also, the measured

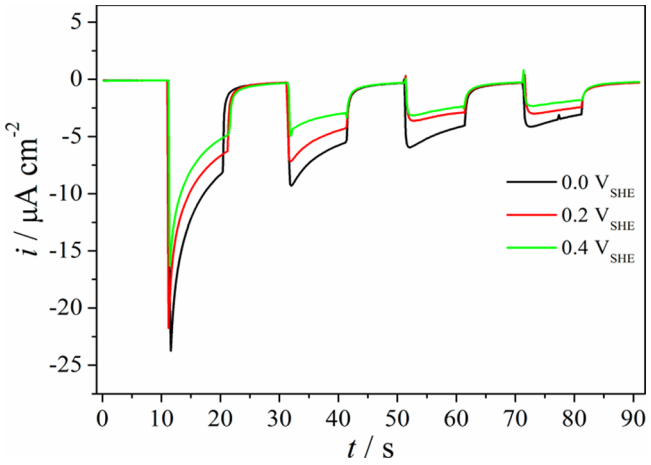

Figure 8. Photocurrent transients measured under intensity modulated green laser light.

photocurrents are overall decreasing with time due to the photodegradation of the material. Within each illumination cycle, the measured photocurrent is highest at the beginning and is decreasing toward the end of each irradiation period. The strongest decay in photocurrent within each cycle is found for the first exposure cycle and is continuously getting smaller for the following cycles. The dark current after each illumination cycle returns to its initial background value. When increasing the applied potential toward more positive values, the measured photocurrent becomes smaller for all experiments. This can be explained by the system being brought closer to flat-band conditions, thereby decreasing the electric field inside the space-charge region. A decreased electric field is less efficient at separating excited electron–hole pairs, resulting in lower photocurrents.

To study the long-term stability of the polymer under irradiation, photocurrent transients were measured for 600 s during illumination with the green laser light at different potentials. The same potentials of 0.0, 0.2, and 0.4 V used in the previous irradiation/dark sequence analysis were also applied here to enable a direct comparison. The measured current transients are shown in Figure 9, and the 600 s exposure time interval is indicated in the figure. The initial dark current densities are shown in the figure before opening the

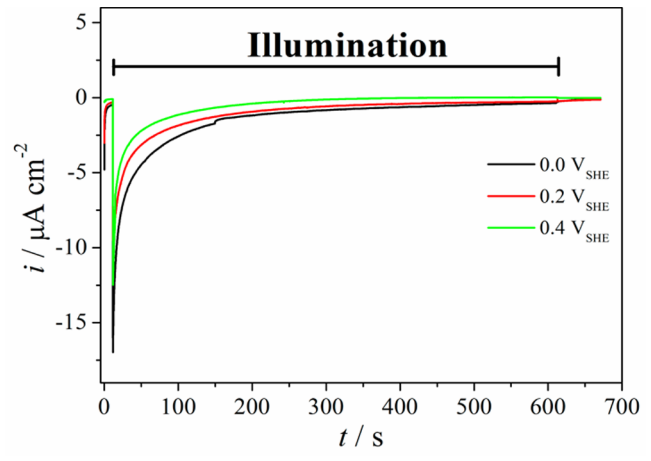

Figure 9. Photocurrent transients measured for 600 s during illumination with green laser.

dx.doi.org/10.1021/jp500423a | J. Phys. Chem. C 2014, 118, 16919–16926

optical shutter in order to indicate the current density background (dark) level. Immediately after opening, the shutter allowing laser irradiation of the MDMO-PPV/electrolyte interface, the maximum in photocurrent is observed for all applied potentials. Within the next 200 s, the photocurrent drops to less than 15% of its initial maximum value. Afterward, the photocurrents are slowly decreasing until approaching the initial dark current. After 600 s of illumination, no clear distinction can be done anymore between photo- and dark current. Therefore, it may be concluded that this polymer suffers from severe photodegradation when being in contact with $TBAPF_6$ electrolyte. As already previously observed in Figure 8, the photocurrent is lower when shifting the applied potential toward more positive values. This can be explained by a decrease in the space charge region allowing a less efficient exciton separation at the electrochemical interface.

In addition to photocurrent measurements, the photopotential of MDMO-PPV in $TBAPF_6$ electrolyte was measured for 300 s, and the results are shown in Figure 10, as obtained

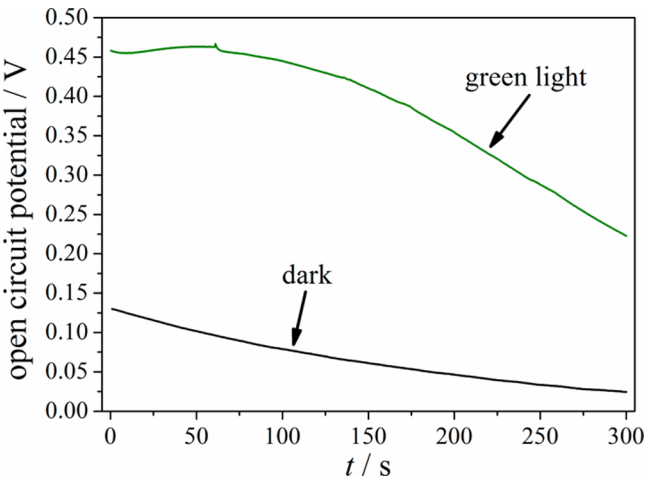

Figure 10. Measured open circuit potential in the dark and under illumination.

from the open circuit potentials measured versus the reference electrode. When a space charge region is present at the semiconducting polymer interface, the photoexcited electrons and holes are separated and each one is moving in opposite direction under the influence of the electric field inside the space charge region. This field-assisted migration of the photoexcited charge carriers induces an opposite potential in the electrode which decreases the potential difference across the space charge region. This reduction further leads to shifting of the Fermi level by a certain energy which can be detected by measuring the photopotential.[28] The electrode potential in the dark continuously decreases from 0.13 V down to 0.05 V. This time variation can be related to the porous nature of the electrode most likely being penetrated more and more by the electrolyte molecules with time. The photopotential measured under green light irradiation stays constant at about 0.46 V for about 50 s and then gradually decreases to 0.22 V within the remaining 250 s of measurement time. However, this decrease is stronger than the decrease of the potential in the absence of irradiation.

4. CONCLUSIONS

A modified version of a photoelectrochemical scanning droplet cell microscope adapted for use with nonaqueous electrolytes is presented. The possibility for localized measurements on single addressed small areas (0.04 mm^2) on a polymer surface is exploited. The small dimension of the cell allows considerably lower consumption of both electrolyte and studied material, as compared to using conventional electrochemical cells. This advantage is evidenced by a detailed electrochemical and photoelectrochemical characterization of a model organic semiconductor (MDMO-PPV). Two oxidation peaks were found during the cyclic voltammetry studies, which were confirmed by potentiostatic investigations. The characteristics of the oxidation processes were studied using scan rate dependent experiments as well as variable maximum potential applied during the potential scan. A shift of the first oxidation peak was observed and discussed. Electrochemical impedance spectroscopy was successfully performed at the micrometer scale revealing the changes in the film resistance as a function of the applied potential. The photovoltaic response of the MDMO-PPV was studied using the described PE-SDCM under irradiation with 532 nm wavelength. High signal-to-noise ratios (>1000) were obtained during the photocurrent measurements on the addressed spot in a reproducible manner. The photocurrent stability was proven during long time measurements. The photopotential of the electrode was also successfully characterized in order to test the applicability of PE-SDCM for photovoltaic studies.

AUTHOR INFORMATION

Corresponding Author

*E-mail: achimwalter.hassel@jku.at. Phone: +43 732 2468-8701. Fax: +43 732 2468-8905.

Notes

The authors declare no competing financial interest.

ACKNOWLEDGMENTS

We gratefully acknowledge the financial support from Austrian Funds for Advancement of Science (FWF) within the Wittgenstein Prize scheme (Z 222-N19 Solare Energieumwandlung). The financial support of the Austrian Federal Ministry of Economy, Family and Youth and the National Foundation for Research, Technology and Development is gratefully acknowledged (Christian Doppler Laboratory for Combinatorial Oxide Chemistry - COMBOX).

REFERENCES

(1) Heeger, A. J.; Sariciftci, N. S.; Namdas, E. B. *Semiconducting and Metallic Polymers*; Oxford University Press: Oxford, NY, 2010.

(2) McEvoy, A.; Markvart, T.; Castañer, L. *Solar Cells: Materials, Manufacture and Operation*, 2nd ed.; Elsevier: Amsterdam, 2013.

(3) Poortmans, J.; Arkhipov, V. *Thin Film Solar Cells: Fabrication, Characterization and Applications*; Wiley: Chichester, England, Hoboken, NJ, 2007.

(4) Singh, M.; Haverinen, H. M.; Dhagat, P.; Jabbour, G. E. Inkjet Printing-Process and Its Applications. *Adv. Mater.* **2010**, *22*, 673−685.

(5) Krebs, F. C. Polymer Solar Cell Modules Prepared Using Roll-to-roll Methods: Knife-Over-Edge Coating, Slot-Die Coating and Screen Printing. *Sol. Energy Mater. Sol. Cells* **2009**, *93*, 465−475.

(6) Krebs, F. C.; Tromholt, T.; Jørgensen, M. Upscaling of Polymer Solar Cell Fabrication Using Full Roll-to-Roll Processing. *Nanoscale* **2010**, *2*, 873.

(7) Krebs, F. C. Fabrication and Processing of Polymer Solar Cells: A Review of Printing and Coating Techniques. *Sol. Energy Mater. Sol. Cells* **2009**, *93*, 394−412.
(8) Kaltenbrunner, M.; White, M. S.; Głowacki, E. D.; Sekitani, T.; Someya, T.; Sariciftci, N. S.; Bauer, S. Ultrathin and Lightweight Organic Solar Cells with High Flexibility. *Nat. Comms.* **2012**, *3*, 770.
(9) Henson, Z. B.; Müllen, K.; Bazan, G. C. Design Strategies for Organic Semiconductors Beyond the Molecular Formula. *Nat. Chem.* **2012**, *4*, 699−704.
(10) Zhou, H.; Yang, L.; You, W. Rational Design of High Performance Conjugated Polymers for Organic Solar Cells. *Macromolecules* **2012**, *45*, 607−632.
(11) Beaujuge, P. M.; Fréchet, J. M. J. Molecular Design and Ordering Effects in π-Functional Materials for Transistor and Solar Cell Applications. *J. Am. Chem. Soc.* **2011**, *133*, 20009−20029.
(12) Gasiorowski, J.; Mardare, A. I.; Sariciftci, N. S.; Hassel, A. W. Characterization of Local Electrochemical Doping of High Performance Conjugated Polymer for Photovoltaics Using Scanning Droplet Cell Microscopy. *Electrochim. Acta* **2013**, *113*, 834−839.
(13) Cardona, C. M.; Li, W.; Kaifer, A. E.; Stockdale, D.; Bazan, G. C. Electrochemical Considerations for Determining Absolute Frontier Orbital Energy Levels of Conjugated Polymers for Solar Cell Applications. *Adv. Mater.* **2011**, *23*, 2367−2371.
(14) Orazem, M. E.; Tribollet, B. *Electrochemical Impedance Spectroscopy*; Wiley: Hoboken, N.J, 2008.
(15) de Gryse, R. On the Interpretation of Mott-Schottky Plots Determined at Semiconductor/Electrolyte Systems. *J. Electrochem. Soc.* **1975**, *122*, 711.
(16) Johansson, T.; Mammo, W.; Svensson, M.; Andersson, M. R.; Inganäs, O. Electrochemical Bandgaps of Substituted Polythiophenes. *J. Mater. Chem.* **2003**, *13*, 1316.
(17) Petr, A.; Dunsch, L.; Neudeck, A. In Situ UV-Vis ESR Spectroelectrochemistry. *J. Electroanal. Chem.* **1996**, *412*, 153−158.
(18) Meisterle, P.; Kuzmany, H.; Nauer, G. In Situ Raman Spectroscopy of the Electrochemical Doping Process in Polyacetylene. *Phys. Rev. B* **1984**, *29*, 6008−6011.
(19) Neugebauer, H. In Situ Vibrational Spectroscopy of Conducting Polymer Electrodes. *Macromol. Symp.* **1995**, *94*, 61−73.
(20) Klod, S.; Ziegs, F.; Dunsch, L. In Situ NMR Spectroelectrochemistry of Higher Sensitivity by Large Scale Electrodes. *Anal. Chem.* **2009**, *81*, 10262−10267.
(21) Dunsch, L. Recent Advances in In Situ Multi-Spectroelectrochemistry. *J. Solid State Electrochem.* **2011**, *15*, 1631−1646.
(22) Gasiorowski, J.; Kollender, J. P.; Hingerl, K.; Sariciftci, S. N.; Mardare, A. I.; Hassel, A. W. Photoelectrochemical Scanning Droplet Cell Microscopy for Localized Photovoltaic Investigations on Organic Semiconductors. *Phys. Chem. Chem. Phys.* **2014**, *16*, 3739−3748.
(23) Hoppe, H.; Glatzel, T.; Niggemann, M.; Schwinger, W.; Schaeffler, F.; Hinsch, A.; Lux-Steiner, M. Ch.; Sariciftci, N. S. Efficiency Limiting Morphological Factors of MDMO-PPV:PCBM Plastic Solar Cells. *Thin Solid Films* **2006**, *511−512*, 587−592.
(24) Gasiorowski, J.; Hingerl, K.; Menon, R.; Plach, T.; Neugebauer, H.; Wiesauer, K.; Yumusak, C.; Sariciftci, N. S. Dielectric Function of Undoped and Doped Poly[2-methoxy-5-(3′,7′-dimethyloctyloxy)-1,4-phenylene-vinylene] by Ellipsometry in a Wide Spectral Range. *J. Phys. Chem. C* **2013**, *117*, 22010−22016.
(25) Hassel, A. W.; Fushimi, K.; Seo, M. An Agar-Based Silver|Silver Chloride Reference Electrode for Use in Micro-Electrochemistry. *Electrochem. Commun.* **1999**, *1*, 180−183.
(26) Morrison, S. R. *Electrochemistry at Semiconductor and Oxidized Metal Electrodes*; Plenum Press: New York, 1980.
(27) Bard, A. J.; Stratmann, M. *Encyclopedia of Electrochemistry*; Wiley-VCH: Weinheim, 2001.
(28) Sato, N. *Electrochemistry at Metal and Semiconductor Electrodes*; Elsevier: Amsterdam, NY, 1998.